One-dimensional vibrations and disorder: The $Zr_{1-x}Hf_xS_3$ solid solution

A. Ait-Ouali, S. Jandl, and P. Marinier
Département de Physique and Centre de Recherche en Physique du Solide, Université de Sherbrooke, Sherbrooke, Québec, Canada J1K 2R1

J.-M. Lopez-Castillo
Département de Médecine Nucléaire et de Radiobiologie, Faculté de Médecine, Université de Sherbrooke, Sherbrooke, Québec, Canada J1H 5N4

A.-M. S. Tremblay
Département de Physique and Centre de Recherche en Physique du Solide, Université de Sherbrooke, Sherbrooke, Québec, Canada J1K 2R1
(Received 29 January 1992; revised manuscript received 1 May 1992)

In the trichalcogenide family of compounds $Zr_{1-x}Hf_xS_3$ there is a frequency range where the optic modes are expected to be describable by a simple one-dimensional model. It is shown that the disorder-induced linewidth in the relevant frequency range could be consistent with theoretical calculations for a simple diatomic chain model. The vibrations involved are along the chain direction and are of B_g type. All the B_g modes of this family of compounds are also here unequivocally identified.

I. INTRODUCTION

Studies of simple one-dimensional models with disorder go back at least as far as Dyson's famous 1953 paper[1] on the disordered harmonic chain. However, from the experimental point of view, real materials with one-dimensional elastic behavior have proven very hard to obtain. The requirement for a crystal to exhibit one-dimensional-like vibrational eigenmodes is clearly to have weak bonding in two directions and strong (covalent) bonding in the other one. This requirement leads in general to structures with complicated unit cells, as is the case for quasi-one-dimensional conductors[2] such as TTF-TCNQ, $(TMTSF)_2X$, etc. It is these complicated unit cells which make the analysis of these compounds difficult, even when some eigenmodes have mainly one-dimensional character. At best one-dimensional vibrations can occur only at special frequencies and in special directions which involve the movement of atoms in the "stiff" direction. Quasi-one-dimensional *electronic* behavior on the other hand (including spin) is observed experimentally[3] in the low-energy properties, but that is in a sense because the Pauli principle can make all the energy levels which contribute to the existence of the real three-dimensional structure irrelevant.

In this paper we study what we believe is the simplest family of compounds where Raman active phonons with one-dimensional character are likely to exist and where it should be quite justified to understand the effect of disorder on one of these one-dimensional phonons with a simple diatomic chain model of the type studied theoretically before. This family is that of the trichalcogenide solid solutions $Zr_{1-x}Hf_xS_3$.

In Sec. II we discuss why the structure of these compounds suggests that phonons with B_g symmetry should have a one-dimensional character. In Sec. III we show experimental evidence from polarized Raman spectra which identify unequivocally the expected four B_g modes. We then proceed in Sec. IV to argue that at least one of these B_g vibrations should be describable by a simple one-dimensional diatomic chain. The possibility of growing structures with Hf and Zr in differing proportions then offers a unique possibility of studying experimentally a disordered one-dimensional diatomic chain. Comparison of the calculated disorder-induced linewidth and the experimentally observed one suggests that one cannot reject the hypothesis that this family of compounds behaves, in the frequency range corresponding to this B_g mode, like a simple disordered diatomic chain. The calculation of the linewidths is based on sum-rule techniques introduced before[4] but which we generalize to apply to the particular class of compounds of interest here. Details of this and other generalizations of the sum rules are given in the Appendix.

II. STRUCTURAL PROPERTIES AND EIGENMODES WITH A ONE-DIMENSIONAL CHARACTER

The structure of the trichalcogenides HfS_3 and ZrS_3 exhibited in Fig. 1 has an unusual anisotropy.[5] These crystals grow with the metal ions in the center of distorted trigonal prisms which share trigonal faces forming isolated chains. The monoclinic unit cell of C_{2h} point group symmetry contains *two* molecular units of adjacent chains which are displaced along the chain axis by half the distance between two metal ions. This leads to the very interesting feature that every one of the nine infrared active modes has a conjugate Raman active mode: In the infrared active modes, the atoms of one chain vibrate in phase with those of the other chain, while they vibrate

 ©1992 The American Physical Society

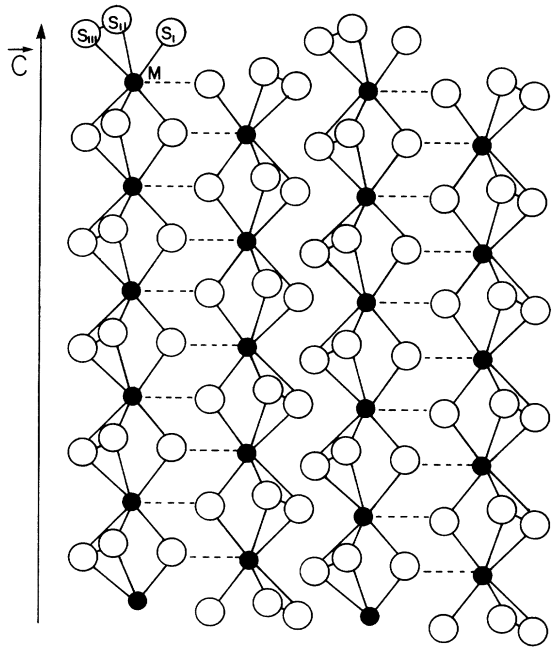

FIG. 1. Crystallographic structure of MS_3 where M=Zr or Hf.

out of phase in the corresponding Raman active modes. There are also three Raman active modes without corresponding infrared ones, for a total of twelve Raman modes. Of these, eight are Ag modes, and four are Bg modes, which correspond, respectively, to vibrations perpendicular and parallel to the chain direction.

In spite of the fibrous aspect of these materials that would suggest strong bonding along the chain direction, and weak bonding in the other two directions, conflicting models were reported concerning the strength of interchain interactions following Raman and infrared measurements.[6-20] By comparing the frequencies of Raman and infrared conjugate modes, Jandl and co-workers[6,7] concluded that eigenmodes had a one-dimensional character whether they were polarized parallel or perpendicular to the chain direction. Grisel and co-workers[13,14] used valence-force and central-force models based on Raman and infrared data showing that vibrations parallel to the chains (B_g) are almost unaffected by the interchain coupling in contrast to the vibrations perpendicular to the chains (A_g). Finally Sourisseau and Mathey,[15] who proposed a valence-force-field model, concluded that interchain and intrachain interactions are comparable. The discrepancies in the calculated force constants of different models comes from the fact that results of model calculations depend on the assignment of the modes' eigenvectors. In the low-symmetry crystal structure of ZrS_3 and HfS_3, group theory predictions are not stringent enough to determine unequivocally the eigenvectors. Moreover, while the Ag modes' Raman intensity is rather strong, the Bg modes' Raman intensity is weak, making these modes difficult to unequivocally identify.

Since many of the infrared modes are difficult to detect for this class of compounds, the present paper concentrates instead on a detailed study of the Raman modes. We stress that the double-chain structure explained above is important to understand why we can even think of applying the disordered diatomic chain model to explain a Raman mode despite the fact that the diatomic chain by itself has only infrared-active modes, not Raman ones: This is possible because the Raman modes of interest are very close in frequency to the corresponding infrared ones, implying weak coupling between chains and hence similar behavior in both spectroscopies.

III. EXPERIMENTAL PROCEDURE AND RESULTS

The dimensions of the monocrystalline samples used in the present work were about 10 mm×2 mm×30 μm. Crystals were grown by iodine chemical transport reaction, taking advantage of the complete range of solid solubility. Even though the lattice parameters a, b, and c do not change significantly throughout the composition, x-ray diffraction permitted a precise determination of x by comparing the intensity of the structure factor $S(001)$ (Ref. 21) for the various compounds.

Raman spectra of 1.6-cm^{-1} resolution in the range 10–550 cm^{-1} were taken at 30 K with the 6471-Å Krypton line laser selected in order to reduce absorption and resonance effects. While low-power radiation impinged on the samples, Raman signals were maximized by using cylindrical lenses and scattering geometries that reduce the background of elastic scattering. Using different orientations of incident and scattered polarizations and taking the Z direction parallel to the chains, both the Ag modes (XX,XY,ZZ) and the Bg modes (XZ,YZ) were detected.

Raman spectra of the Ag (XX) and Bg (XZ) modes of $Zr_{1-x}Hf_xS_3$ are presented, respectively, in Figs. 2(a) and 2(b) and Figs. 3(a) and 3(b) with an x increment of 0.1. In Fig. 4, mode frequencies are plotted as a function of x while the evolution of the phonon linewidth with composition is illustrated in Figs. 5(a)–5(c) for the Bg modes and in Fig. 6 for the Ag modes. As shown in Table I, there are some discrepancies in the reported frequencies of the end members ZrS_3 and HfS_3 partly due to the strong intensity of the Ag modes and the weak intensity of the Bg modes. The latter can easily be masked by a strong Ag phonon or by a local (impurity) mode. Our measurements permit unequivocal identifications of the Bg and Ag modes through their evolution in the solid solution. In Fig. 4, the full lines 1–8 represent the evolution of the Ag modes: lines 9–12 stand for the Bg modes while dashed lines represent either local modes, zone edge modes, second-order modes (286+80=366, 286+27=313, 236+27=263 all in cm^{-1}), or isotopic (518 cm^{-1}) modes.[15]

The interpretation of the spectra was facilitated by the fact that the degeneracy of the 153-cm^{-1} Ag and Bg modes (lines 5 and 9) is lifted for high Hafnium content in $Zr_{0.2}Hf_{0.8}S_3$ as in ZrS_3 under hydrostatic pressure.[22,23] With the lifting of degeneracy, the presence of a third peak reported in the powder study[20] is not observed.

The four Bg modes predicted by group theory have their frequencies within the range 140–265 cm^{-1}. As

displayed in Fig. 4, they exhibit one-mode behavior, in other words, the corresponding line shape has a single maximum which appears to gradually shift with composition.[24] They were difficult to identify in previous studies of ZrS_3 (Refs. 15, 17, and 25) and HfS_3 (Ref. 18) as well as in polycrystalline $Zr_{1-x}Hf_xS_3$, where they were reported erroneously to mix and to exhibit a two-mode-type behavior.[20]

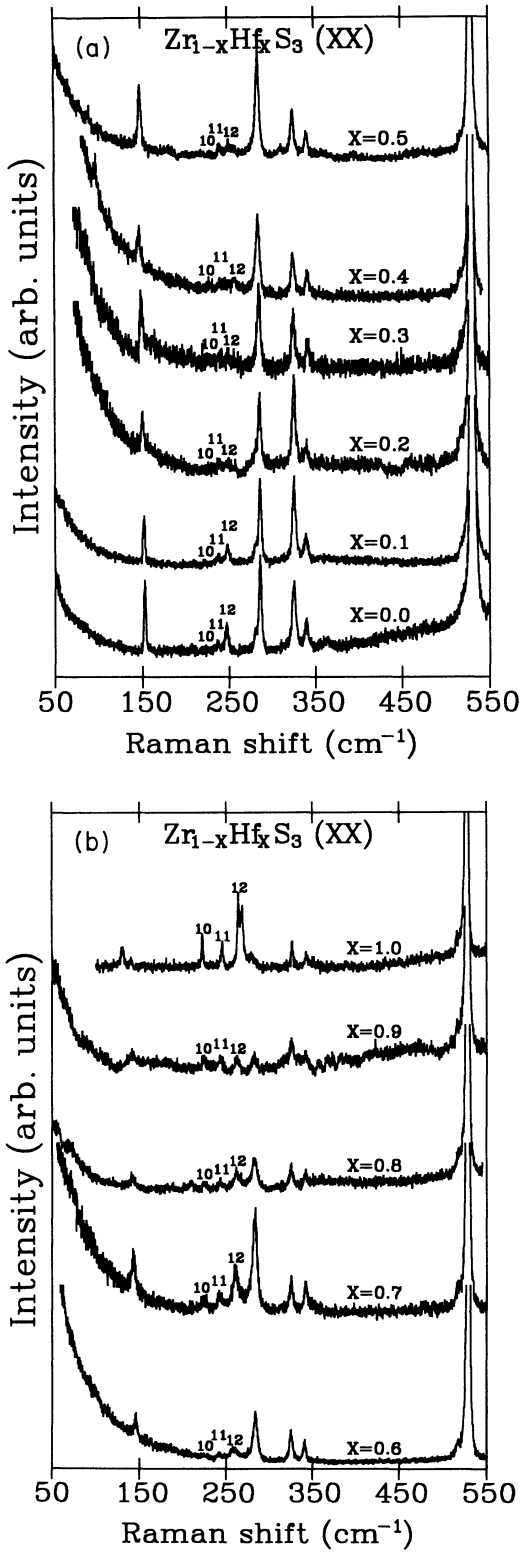

FIG. 2. Polarized Raman spectra (XX) of $Zr_{1-x}Hf_xS_3$ at 30 K with an x increment of 0.1.

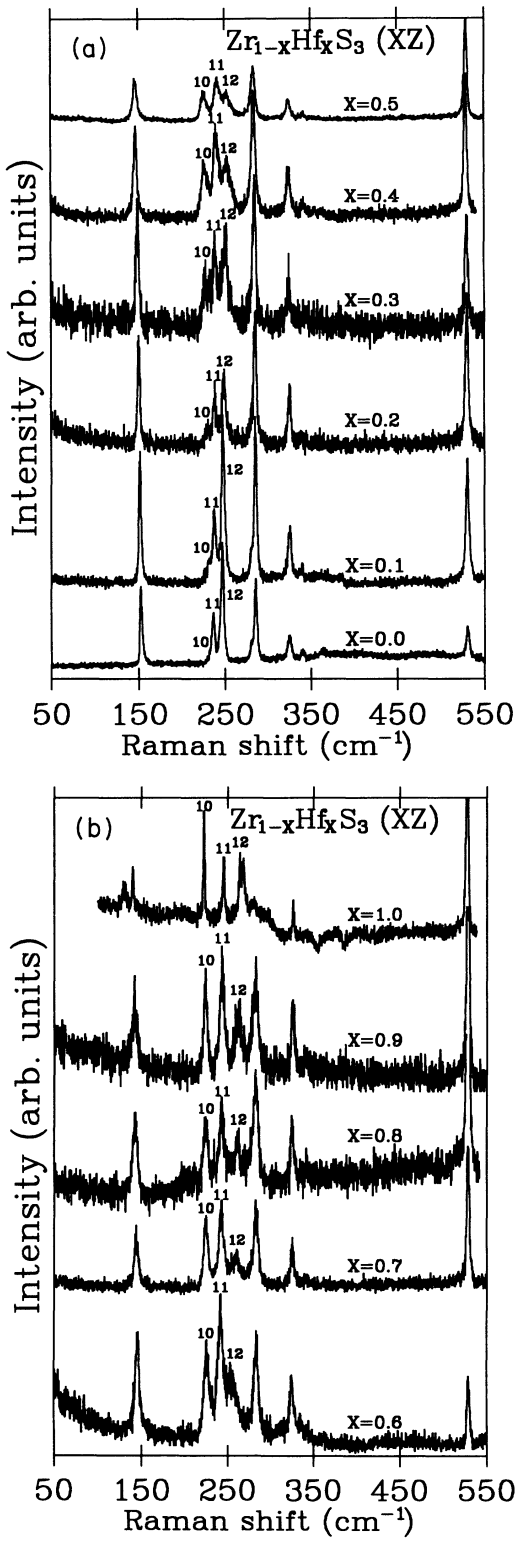

FIG. 3. Polarized Raman spectra (XY) of $Zr_{1-x}Hf_xS_3$ at 30 K with an x increment of 0.1.

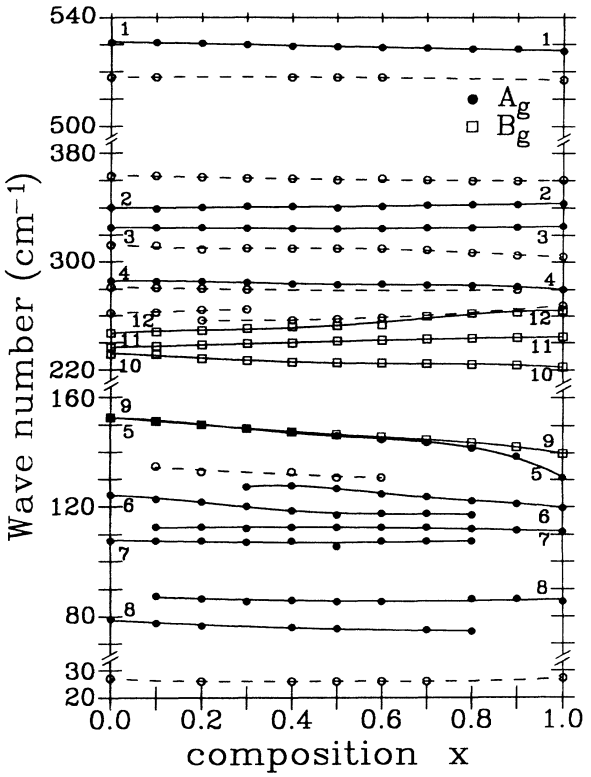

FIG. 4. Mode wave numbers of $Zr_{1-x}Hf_xS_3$ as a function of compositional parameter x. The curves are guides for the eye. Lines have been numbered from 1 to 8 for Ag modes and 9 to 12 for Bg modes corresponding to the labeling in Figs. 2 and 3.

IV. DISORDER-INDUCED LINEWIDTHS: THEORETICAL PREDICTIONS FOR THE SIMPLE DIATOMIC CHAIN VERSUS EXPERIMENT

Given the structural properties discussed in Sec. II, it appears reasonable to hypothesize that the four Bg modes (corresponding to vibrations parallel to the chain direction) behave as if they were on a one-dimensional structure. In this case, the Bg mode where the S_3 complex moves against the metal ion as a rigid molecule[26] is expected to behave as the optic mode of a simple disordered diatomic chain[27–29,4] $AB_{1-x}C_x$. The A ion would stand for the S_3 complex, and B and C for Zr and Hf. To be able to apply the diatomic chain model, elementary considerations of perturbation theory indicate that it is important to have no other optic mode near the frequency range determined by the frequency of the mode in pure ZrS_3 and that in pure HfS_3.

In this section we show that one cannot reject the hypothesis that there is a frequency range where the disordered diatomic chain $AB_{1-x}C_x$ model is applicable. Indeed, we find that the observed disorder-induced linewidth, in the appropriate frequency range of the real compounds, behaves as predicted under the simplest theoretical assumptions.

The theoretical prediction for the disorder-induced linewidth is obtained from a simple generalization of Ref. 4, which considers not only mass disorder, but also force constant disorder. In Ref. 4, the scattered intensity is normalized to unity and sum rules are used to compute various moments of the intensity distribution. These moments are averages of ω^{2n} over the normalized intensity distribution and they are obtained analytically. When the observed scattered intensity is concentrated around a single maximum, these moments can be used to estimate the position of the maximum, as well as the width of the intensity distribution as a function of disorder.

Taking a one-dimensional chain model with nearest-neighbor force constants and longitudinal vibrations, the known atomic masses and the observed frequencies in the pure compounds completely determine the force constant, k_{Hf}, between Hf and the S_3 cage, as well as the corresponding quantity, k_{Zr}, in the Zr case. Hence there is no adjustable parameter in the calculations. It is assumed, however, that the probability of occupation of a metallic site by either Zr or Hf is independent of the occupation of the neighboring sites (the site occupations are independently distributed random variables). In the Appendix, the reader will find more details along with generalizations of our results to the case where there is polarizability disorder as well as correlations. In the simplest case discussed above, the position of the maximum of the spectral intensity, $\omega(x)$, may be estimated from the moments of the intensity distribution. The result is given by

$$\omega(x)=\left[\frac{x_{Zr}k_{Hf}\omega_{Zr}^4+x_{Hf}k_{Zr}\omega_{Hf}^4}{x_{Zr}k_{Hf}\omega_{Zr}^2+x_{Hf}k_{Zr}\omega_{Hf}^2}\right]^{1/2}, \tag{1}$$

where the concentration x in $Zr_{1-x}Hf_xS_3$ is used to define the occupation probabilities $x_{Hf}=x$ and $x_{Zr}=1-x$, while ω_{Zr} and ω_{Hf} are the zone center optic frequencies of the corresponding pure compounds, ZrS_3 and HfS_3:

$$\omega_{Hf}^2=2k_{Hf}(m_{S_3}^{-1}+m_{Hf}^{-1}),\quad \omega_{Zr}^2=2k_{Zr}(m_{S_3}^{-1}+m_{Zr}^{-1}). \tag{2}$$

In this model, we recall that the triangle made of the three sulfurs is considered as a single atom so that $m_{S_3}=3m_S$. Defining

$$\Delta\omega^2=\omega_{Hf}^2-\omega_{Zr}^2, \tag{3}$$

the expression (1) for the concentration dependence of the frequency takes a simple form in the limit $\Delta\omega^2/\omega_{Zr}^2\ll 1$ and $(k_{Hf}-k_{Zr})/k_{Zr}\ll 1$, appropriate for the present experiment:

$$\omega(x)\approx\omega_{Zr}+x(\omega_{Hf}-\omega_{Zr}). \tag{4}$$

The result for the linewidth as a function of disorder is estimated by the standard deviation $\delta\omega^2$. One obtains in the Appendix,

$$\delta\omega^2(x)=\frac{(x_{\mathrm{Zr}}x_{\mathrm{Hf}})^{1/2}|\Delta\omega^2|}{x_{\mathrm{Zr}}\omega_{\mathrm{Zr}}^2k_{\mathrm{Zr}}^{-1}+x_{\mathrm{Hf}}\omega_{\mathrm{Hf}}^2k_{\mathrm{Hf}}^{-1}}\left[\frac{\omega_{\mathrm{Zr}}^2\omega_{\mathrm{Hf}}^2}{k_{\mathrm{Zr}}k_{\mathrm{Hf}}}-\frac{1}{m_{s_3}}(x_{\mathrm{Zr}}\omega_{\mathrm{Zr}}^2k_{\mathrm{Zr}}^{-1}+x_{\mathrm{Hf}}\omega_{\mathrm{Hf}}^2k_{\mathrm{Hf}}^{-1})\right]^{1/2}, \tag{5}$$

from which it is easy to extract $\delta\omega=(\delta\omega^2)/(2\omega)$. The leading dependence on disorder comes from the $x_{\mathrm{Zr}}x_{\mathrm{Hf}}=x(1-x)$ prefactor in Eq. (5). Since this result is based on a purely harmonic model, the linewidth vanishes for the two pure compounds. However, we know that there is an intrinsic width to the lines, mainly due to anharmonicities. This effect is included in the most simple manner by adding to $\delta\omega^2(x)$ above, the following broadening:

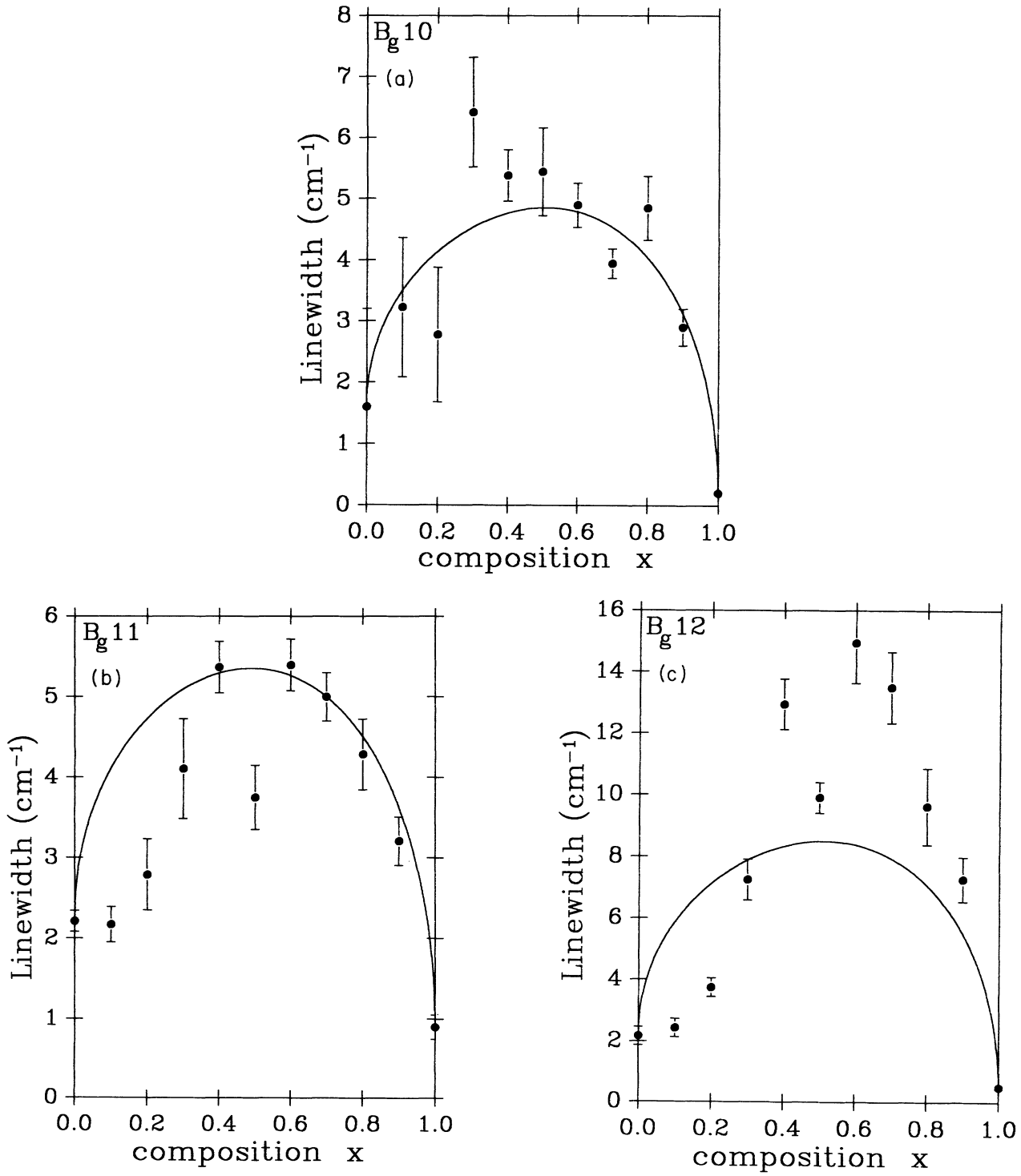

FIG. 5. (a), (b), and (c): Mode linewidths for, respectively, the Bg modes numbered 10, 11, and 12 as a function of compositional parameter x. The curves are the theoretical ones using Eq. (5) with the anharmonic linewidth given by Eq. (6).

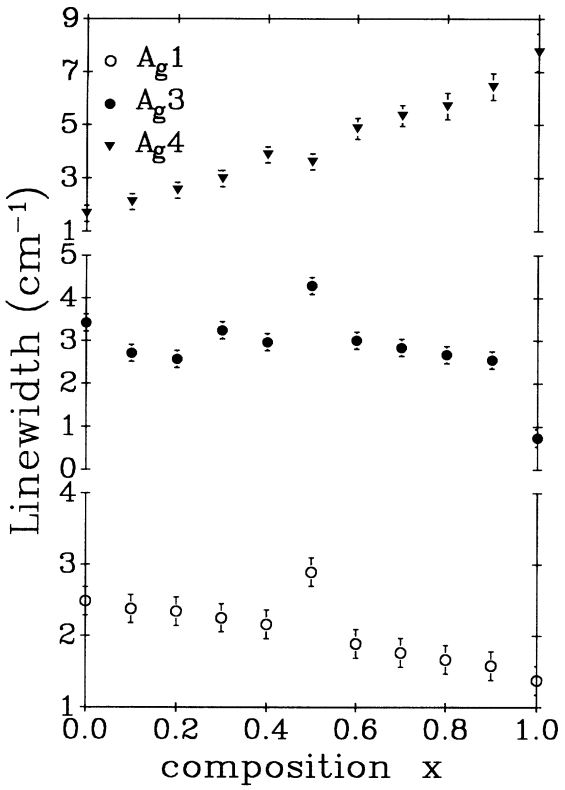

FIG. 6. Mode linewidths of the Ag modes numbered 1, 3, and 4 as a function of compositional parameter x.

$$\delta\omega_{\rm an}^2(x)=x\delta\omega_{\rm Hf}^2+(1-x)\delta\omega_{\rm Zr}^2 , \tag{6}$$

where $\delta\omega_{\rm Hf}^2$ and $\delta\omega_{\rm Zr}^2$ are obtained respectively from the observed linewidths of the pure compounds, assuming a Lorentzian line shape. The precise dependence on x of $\delta\omega_{\rm an}^2$ should not influence the results too much since the anharmonic linewidth is usually much smaller than the disorder-induced linewidth. Note, however, that while this is a reasonable assumption for Hf-rich compounds, the Zr-rich compounds have an intrinsic linewidth comparable to the disorder-induced one in some of the cases of interest.

As stated before, the results just obtained will be useful to estimate experimental spectral properties such as position of the maximum and linewidth, only when the spectral intensity is centered around a single frequency. Whether this is the case or not cannot be decided by sum rules alone. Furthermore, to relate $\delta\omega$ to a linewidth, one has to know the line shape since there are usually numerical factors relating, for example, standard deviation to the full width at half height. We thus performed numerical simulations for the disordered diatomic chain $AB_{1-x}C_x$ with about 3×10^5 ions per chain: The contribution of each eigenmode to the spectral intensity was proportional to the square of the projection of its eigenvector on the $\mathbf{k}=0$ vector with respective value 1 and -1 for the two ions in the basic unit cell. Each eigenmode has an intrinsic width which is modeled as in Eq. (6). The simulations allowed us to verify that over the whole range of concentrations one obtains one-mode-type behavior, meaning that the spectral intensity is centered around a single frequency.

For illustrative purposes, we show in Fig. 7 the results of the simulation for the case $x=0.6$ as well as the same results convoluted with a Lorentzian of width 1.6 cm^{-1} to illustrate what this model would predict (dashed line) for the appearance of experimental raw data. Clearly, while there are asymmetries in the bare calculated line shape, the convolution makes this less apparent.

We are now ready to make comparisons with experiment. First we consider the shift of the phonon position with disorder. The four Bg frequency shifts, as well as those of the one-mode Ag phonons (lines 1, 2, 3, and 4 of Fig. 4), clearly all satisfy Eq. (4) for the disorder-induced frequency shift. Given the small shifts and the experimental precision, it is not possible to make more detailed comparisons with the more precise formula (1) for the shift. This frequency shift then is not a sensitive test.

A more stringent test of the theoretical model is to compare the linewidths with experiment. Since the prime candidates for behaving in a one-dimensional manner are the four Bg modes, their linewidths are plotted as a function of composition x in Figs. 5(a), 5(b), and 5(c). These linewidths correspond, respectively, to the Bg phonons whose frequency positions appear in lines 10, 11, and 12 of Fig. 4. Line 9 was disregarded because it is masked by line 5. (Even though the latter is an Ag phonon, it is strong enough to leave traces in the Bg scattering configuration.)

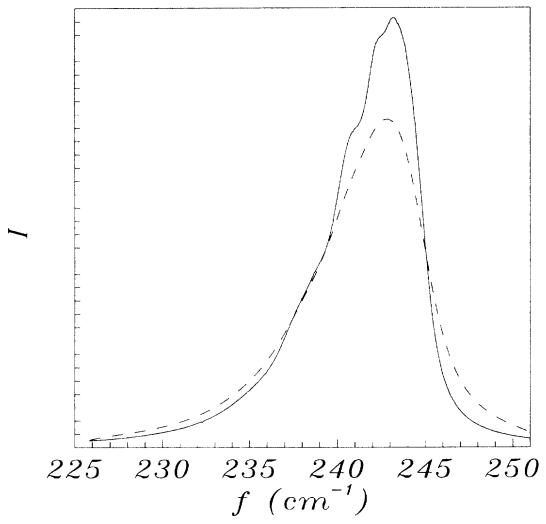

FIG. 7. Results of a simulation for the scattered intensity in the case $x=0.6$ with values of the parameters determined from the known atomic masses and measured eigenfrequencies and linewidths in the pure compounds: $\nu_{\rm Zr}=236.2$ cm^{-1}, $\nu_{\rm Hf}=245.3$ cm^{-1}, $\delta\nu_{\rm Zr}=2.2$ cm^{-1}, $\delta\nu_{\rm Hf}=0.899$ cm^{-1}. The number of ions is of order 3×10^5. The dashed line is the convolution of the results represented by the solid line with a Lorentzian of width 1.6 cm^{-1}.

TABLE I. Observed wave numbers and symmetries for $\mathbf{k}=\mathbf{0}$ Raman modes in ZrS_3 and HfS_3.

ZrS_3										HfS_3									
Ref. 13 (300 K)		Ref. 15 (300 K)		Ref. 25 (300 K)		Ref. 17 (300 K)		This work (30 K)		Ref. 13 (300 K)		Ref. 19 (300 K)		Ref. 18 (300 K)		This work (30 K)	
ν (cm^{-1})	Sym.	ν (cm^{-1})	Sym.	ν (cm^{-1})	Sym.	ν (cm^{-1})	Sym.	ν (cm^{-1})	Sym.	ν (cm^{-1})	Sym.	ν (cm^{-1})	Sym.	ν (cm^{-1})	Sym.	ν (cm^{-1})	Sym.
21	A_g	19	Imp.	21	Imp.			27	Imp.	15	A_g	17	A_g			27	Imp.
		84	A_g	83	A_g	84	A_g	80	A_g	73	A_g	74	A_g	73	A_g	86	A_g
110	A_g	108	B_g	108	A_g			108	A_g			111	A_g	111	A_g	111	A_g
		122	A_g	123	A_g	122	A_g	124.5	A_g							120	A_g
151	A_g	150	A_g	150	A_g	140	B_g	153	A_g	127	A_g	130	A_g	128	A_g	131	A_g
152	B_g			150	B_g	150	A_g	153	B_g	140	B_g	140.5	B_g	140	B_g	140	B_g
		234	B_g	237	B_g	234	B_g	232	B_g			218	B_g	219	B_g	222.5	B_g
		243	B_g	243	B_g	242	B_g	236.5	B_g			246	B_g	246	B_g	245.5	B_g
								247	B_g							264.5	B_g
		260						262		261	A_g	260	A_g	261	A_g	268	
		(150+108)						(236+27)				264	A_g			(245+27)	
		275	A_g	275	A_g	275	A_g	281	Should								
282	A_g	280	A_g	281	A_g	281	A_g	286	A_g			275	A_g	275	A_g	280	A_g
								313								303	
								(286+27)								(280+27)	
322	A_g	320	A_g	320	A_g	321	A_g	325	A_g	322	A_g	322	A_g	322	A_g B_g	326.5	A_g
		330	B_g	333	A_g	330	B_g	340	A_g			340	A_g	339	A_g	343	A_g
		360						363								360	
								(286+80)								(280+86)	
		516	Isot.					518	Isot.							517	Isot.
		527	A_g	529	A_g	529	A_g	531	A_g	524	A_g	525.5	A_g	526	A_g	527.5	A_g

To make a direct comparison with theory, one should evaluate the standard deviation of the normalized experimental intensity. Unfortunately, this is not possible because of background and because of the presence of many phonon lines. Experimental linewidths were obtained instead by fitting a Lorentzian to the phonon peaks and subtracting 1.6 cm^{-1} to account for the spectrometer response, which is also Lorentzian. Since the full width at half maximum is related to the standard deviation through a constant factor which depends on the particular disorder-induced line shape, we resort again to simulations to find out how to compare full widths at half maximum with analytically computed standard deviation. Taking simply the full width at half maximum of the simulated scattered intensity gives a result which, as in Ref. 4, agrees qualitatively with $\delta\nu \equiv \delta\omega/(2\pi)$ as calculated from sum rules. More specifically, the full width at half maximum of the simulations is smaller than the prediction obtained from $\delta\nu$ when x is large, while the opposite is true when x is small. *We thus compare experimental linewidths directly to* $\delta\nu$*, this being the main assumption of the present work.* In the case of simulations, the full width at half maximum may differ from $\delta\nu$ by a very large percentage.

While all Bg modes are perhaps describable by a one-dimensional model, three of them certainly involve movements of the sulfur atoms with respect to each other. For these cases, one expects to need at least one-dimensional models with more atoms per unit cell than the simple diatomic-chain model described above. Comparing the theoretical prediction of Eq. (5) [including the anharmonicity Eq. (6)], shown in Figs. 5(a)–5(c) as a solid line, one finds that the linewidth of mode 12 [Figs. 4 and 5(c)], agrees only qualitatively with the theoretical prediction while the Bg modes 10 and 11 of Figs. 5(a) and 5(b) might both be describable by the disordered diatomic chain. In Fig. 5(b) (Bg mode 11), the narrowing of the linewidth for $x=0.5$ might reflect some ordering within the chains at this commensurate fraction, as occurs in other compounds such as $Ga_xIn_{1-x}P$.[30,31] The corresponding *increase* in linewidth of the Ag vibrations could indicate that disorder persists from chain to chain. The fact that the disagreement between theory and experiment for either of the two Bg modes 10 and 11 is mainly in the region $x<0.5$ may have several causes, the most likely one being the proximity of the two Bg modes (10 and 11 in Fig. 4) for small x. A look at the spectra in Figs. 3(a) and 3(b) clearly shows that, for small x, the separation of these modes is comparable to their linewidths, which means that they certainly interact strongly. This violates the requirement for applicability of the diatomic-chain model that the optic mode should be isolated from other modes in the relevant frequency range.

Note that not only mode 11, but all other Bg modes are narrower than expected for $x<0.5$. The simulations tend to be narrower than the sum-rule prediction for large x (Hf-rich compositions) instead of small x. We must also investigate the possibility that Hf does not mix very well in Zr-rich compounds. To check this hypothesis, analytical results are presented in the Appendix for the case where the joint probability for having neighboring metallic atoms of the same kind is arbitrary. With very large joint probability for clustering, the linewidth does decrease, but not enough. To explain the observed linewidths, we would probably need very large cluster sizes, at least for the $x=0.1$ and $x=0.2$ compounds. Finally, note that we have assumed that anharmonicities do not interfere with disorder.

While mode 10 is the one with the best overall agreement between theory and experiment, in fact we would have expected the Bg mode with lowest frequency to be the one which compares well with the simple diatomic chain: Indeed, fewer chemical bonds are involved when the sulfurs are not moving with respect to each other. This lowest-frequency Bg mode is No. 9 in Fig. 4, and its width is inaccessible because of the Ag mode as explained earlier. Nevertheless, overall qualitative agreement of the three other Bg mode linewidths with the simplest $AB_{1-x}C_x$ one-dimensional model could result if strong metal-ion–chalcogen bonds render the effect of out-of-phase sulfur vibrations irrelevant to the disorder-induced linewidth. This is suggested by the better agreement with theory for the Hf-rich compounds, which have a stronger metal-ion–chalcogen bond than Zr-rich compounds (as shown by the fact that the mode frequency is almost unchanged as the concentration x varies, despite the large mass increase in going from Zr- to Hf-rich compounds).

Finally, Fig. 6 shows the evolution of the Ag one-mode phonon linewidths with composition for lines 1, 3, and 4 of Fig. 4. The behavior is clearly different in the case of the Ag phonon linewidths since the inverted-parabola shape observed for the Bg linewidth as a function of composition is replaced by a linear monotonic variation. Two reasons for this could be invoked: (a) The most likely one is that these vibrations perpendicular to the chain involve force constants which are comparable to those along the chain. This would be in agreement with the calculations of Griesel and co-workers[13,14] and a purely one-dimensional model could not apply for these modes. (b) The eigenvectors associated to these high-frequency Ag modes cannot be approximated by the vibrations of the diatomic chain (even though they may be one-dimensional).

V. CONCLUSION

Our main result is the agreement, illustrated in Fig. 5(a), between the linewidth of one Bg mode of $Zr_{1-x}Hf_xS_3$ and a calculation of this linewidth based on a sum-rule approach for a one-dimensional disordered diatomic chain $AB_{1-x}C_x$ with A repeated every other atom. The calculation is for an infrared mode while experiment in Fig. 5(a) is for a Raman mode, but the weak coupling between the two chains within a unit cell leads one to expect similar results in both spectroscopies. However, we had to make one strong assumption, namely that the full width at half maximum of the experimental line can be compared with the standard deviation obtained from sum rules. This assumption depends on the line shape, which we cannot predict analytically. Simulations on the simple diatomic chain indicate that this assumption can be incorrect by a large percentage for the

diatomic-chain model without anharmonicity. However, depending on concentration, the line shape from simulations can be larger or smaller than the sum-rule result, and on average the trends from sum rules and from simulations are the same. We can speculate that in the real system anharmonicities make the line shape smoother than in the simulations, leading to a better agreement with sum rules. Finally, within the resulting uncertainties, either of the two Bg modes in Figs. 5(a) and 5(b) could be good candidates for a diatomic-chain description.

From the experimental point of view, this work allows unequivocal identification of the four Bg modes predicted by group theory. Indeed, the evolution of their linewidth with composition confirms the symmetry assignment since for Bg modes one observes a paraboliclike behavior very different from the almost linear dependence of the Ag modes.

Despite many years of theoretical studies on the one-dimensional harmonic chain, there seem to be very few experimental realizations of this model. We have shown that $Zr_{1-x}Hf_xS_3$ is a case where there is a frequency range for which a one-dimensional model with a simple unit cell is not an inconsistent model. Comparisons with other theoretical results, such as the island-frequency[32] problem, would, however, necessitate these compounds to have smaller intrinsic (anharmonic) linewidths.

ACKNOWLEDGMENTS

The help of M. Parenteau in fitting the Raman spectra is gratefully acknowledged. One of us (A.A.-O.) acknowledges the financial support of the Algerian government. This work was supported by the Natural Sciences and Engineering Research Council of Canada (NSERC) and the Fonds pour la Formation de Chercheurs et l'Aide à la Recherche from the Government of Québec.

APPENDIX: SUM RULES FOR VARIOUS TYPES OF DISORDER

In Ref. 4, analytical results were given for the case of uncorrelated mass disorder only. In the following, using the same notations, we present results for three cases: (a) uncorrelated mass and force-constant disorder; (b) correlated mass and force-constant disorder; (c) Correlated mass, force-constant, and coupling-constant (or intensity) disorder. In all cases we consider the $AB_{1-x}C_x$ chain. In other words, the pure binary chain AB is diluted by replacing the B ion of mass m_B with a C ion of mass m_C, sometimes in an uncorrelated manner, sometimes with correlations. The ion A of mass m_A is still repeated periodically. The force constant k_{AB} between A and B is not the same as the force constant k_{AC} between A and C. The zone center optic frequency ω_{AB} of a pure compound AB is $\omega_{AB}^2=2k_{AB}(m_A^{-1}+m_B^{-1})$. We are interested in the following measure of the linewidth: $\delta\omega^2=[\overline{\omega^4}-(\overline{\omega^2})^2]^{1/2}$, where $\overline{\omega^n}\equiv\omega^{(n)}/\omega^{(0)}$ and the moments $\omega^{(n)}$ are given below for various cases.

(a) Uncorrelated mass and force-constant disorder. No disorder is assumed in the coupling constants, hence without loss of generality we may take, $f_A=1$ and $f_B=f_C=-1$. The occupation probability of a site on the disordered sublattice is independent of the occupation probability of any other site, hence the probability of finding an ion of type C in the disordered sublattice is $x_C\equiv x$, while that of finding an ion of type B is $x_B=(1-x)$. The results for the first three moments are

$$\omega^{(0)}=\frac{1}{4}\left[\frac{x_B\omega_{AB}^2}{k_{AB}}+\frac{x_C\omega_{AC}^2}{k_{AC}}\right], \tag{A1}$$

$$\omega^{(2)}=\frac{1}{4}\left[\frac{x_B\omega_{AB}^4}{k_{AB}}+\frac{x_C\omega_{AC}^4}{k_{AC}}\right], \tag{A2}$$

$$\omega^{(4)}=\frac{1}{4}\left[\frac{x_B\omega_{AB}^6}{k_{AB}}+\frac{x_C\omega_{AC}^6}{k_{AC}}-\frac{x_Bx_C}{m_A}(\omega_{AB}^2-\omega_{AC}^2)^2\right]. \tag{A3}$$

The result for $\delta\omega^2/(2\omega)$ should be equal to the full width at half maximum for a narrow Lorentzian peaked between ω_{AB} and ω_{AC} when $\omega_{AB}\approx\omega_{AC}$. This quantity is plotted as a solid line in Figs. 5(a)–5(c) for the values of parameters appropriate for experiment. It is also plotted as a solid line in Fig. 8 where it is compared with results about to be described.

(b) Correlated mass and force constant disorder. Let p_{BB} the probability of having the sequence of ions BAB on the chain, $p_{BC}=p_{CB}$ for the sequences BAC and CAB and p_{CC} for the sequence CAC. We have the following normalization constraints:

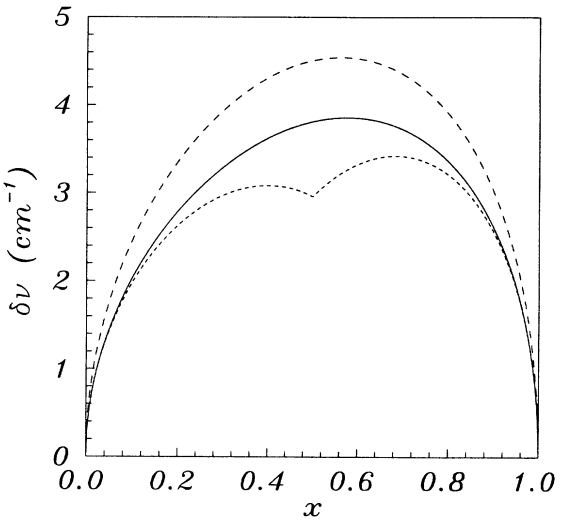

FIG. 8. Analytical results for $\delta\nu=\delta\omega/2\pi=\delta\omega^2/(4\pi\omega)$. For the case of uncorrelated mass and force-constant disorder (solid line), $\delta\omega$ is obtained from Eqs. (A5)–(A8) and (A11)–(A13). The dashed and the short-dashed curves are for the cases where p_{BC} is, respectively, minimum and maximum. The curves are computed from Eqs. (A5)–(A8) and (A11), (A12), and (A15). The kink at $x=0.5$ comes from the fact that maximum p_{BC} at this concentration leads to a pure ternary compound.

$$p_{BB}+2p_{BC}+p_{CC}=1\ ,$$
$$p_{BB}+p_{BC}=x_B\ , \tag{A4}$$
$$p_{CC}+p_{CB}=x_C\ ,$$

two of which are independent. One of the probabilities suffices to determine all the others. Since correlations will have a nontrivial effect only when terms of the type $k_{i-1,i}k_{i,i+1}$ or $m_{i+1}^{-1}m_{i-1}^{-1}$ appear, their effect does not show up in $\omega^{(0)}$ or $\omega^{(2)}$. For $\omega^{(4)}$ we obtain

$$\omega^{(4)}=\frac{1}{4}\left[\frac{x_B\omega_{AB}^6}{k_{AB}}+\frac{x_C\omega_{AC}^6}{k_{AC}}-\frac{p_{BC}}{m_A}(\omega_{AB}^2-\omega_{AC}^2)^2\right]. \tag{A5}$$

In Fig. 8 we plot $\delta\nu=\delta\omega^2/(4\pi\omega)$ for the case of correlations, using (A1), (A2), and (A5). The dashed line is for the case where p_{BC} is minimum ($=0$), and the short-dashed line for the case where p_{BC} is maximum [$=\min(x_B,x_C)$].

(c) Correlated mass, force-constant, and coupling-constant disorder. In the physical problem, the coupling constants f_i are bond properties. Hence, we take as our model $f_A=(f_i+f_j)/2$, with f_i and f_j equal to f_B or f_C depending on the neighbors of A. Since there are only two types of bonds in the lattice, namely AB and AC, this is appropriate. In computing $\omega^{(4)}$, one encounters terms of the form $f_{i+1}k_{i,i+1}f_{i-1}k_{i-1,i}/(m_im_{i-1}m_{i+1})$. When i is an ion of type B, $i+1$ and $i-1$ are of type A, so to know f_{i+1} and f_{i-1} one needs to know whether the sequence of ions is $BABAB$, $CABAB$, or whatever. In other words, we need p_{BBB}, p_{BCB}, etc. Using the normalization and symmetry constraints, the joint probabilities may be expressed in terms of p_{BC}, p_{BCB}, p_{CBC}, and x_B, x_C only. Defining also $\delta f=f_C-f_B$, the results in this case may be written in the form

$$\omega^{(0)}=\frac{1}{4}\left[\frac{x_Bf_B^2\omega_{AB}^2}{k_{AB}}+\frac{x_Cf_C^2\omega_{AC}^2}{k_{AC}}-\frac{p_{BC}\delta f^2}{m_A}\right], \tag{A6}$$

$$\omega^{(2)}=\frac{1}{4}\left\{\frac{x_Bf_B^2\omega_{AB}^4}{k_{AB}}+\frac{x_Cf_C^2\omega_{AC}^4}{k_{AC}}-\frac{p_{BC}}{m_A}\left[\delta f^2\left[\omega_{AB}^2+\omega_{AC}^2-\frac{k_{AB}}{m_A}-\frac{k_{AC}}{m_A}\right]+(\omega_{AB}^2-\omega_{AC}^2)(f_B^2-f_C^2)\right]\right\}, \tag{A7}$$

$$\omega^{(4)}=\frac{1}{4}\left[\frac{x_Bf_B^2\omega_{AB}^6}{k_{AB}}+\frac{x_Cf_C^2\omega_{AC}^6}{k_{AC}}+\frac{p_{BCB}k_{AC}^2\delta f^2}{m_A^2m_C}+\frac{p_{CBC}k_{AB}^2\delta f^2}{m_A^2m_B}\right.$$
$$+\frac{p_{BC}}{m_A}\left\{f_B^2(\omega_{AB}^2-\omega_{AC}^2)\left[\frac{k_{AB}}{m_A}+\frac{k_{AC}}{m_A}-2\omega_{AB}^2-\omega_{AC}^2\right]+f_C^2(\omega_{AC}^2-\omega_{AB}^2)\left[\frac{k_{AB}}{m_A}+\frac{k_{AC}}{m_A}-2\omega_{AC}^2-\omega_{AB}^2\right]\right.$$
$$\left.\left.-\frac{\delta f^2}{2}\left[2(\omega_{AB}^4+\omega_{AC}^4+\omega_{AB}^2\omega_{AC}^2)-\left[\frac{(3k_{AB}+2k_{AC})\omega_{AB}^2+(2k_{AB}+3k_{AC})\omega_{AC}^2}{m_A}\right]+\frac{4k_{AB}k_{AC}}{m_A^2}\right]\right\}\right]. \tag{A8}$$

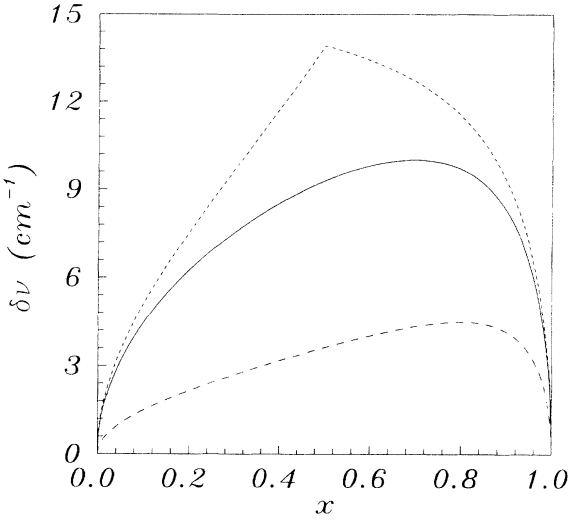

FIG. 9. Analytical results for $\delta\nu=\delta\omega/2\pi=\delta\omega^2/(4\pi\omega)$ in the most general case, including coupling-constant disorder. The dashed and solid lines refer to various degrees of correlations in the disorder, as in Fig. 8: solid line for uncorrelated disorder, dashed line for minimal value of p_{BC}, and short-dashed line for maximal value of p_{BC}. In all three cases, there is the same disorder in the coupling constants: For the bond involving the heavy metal ion, Hf, we take $f_{\mathrm{Hf}}=1$, while for the bond involving the light metal ion, Zr, we take $f_{\mathrm{Zr}}=1.74$. Equations (A5)–(A8) and the general results (A16)–(A18) are used for the calculations.

In Fig. 9, we plot $\delta\nu=\delta\omega/2\pi=\delta\omega^2/(4\pi\omega)$ in the most general case, including coupling-constant disorder. The dashed and solid lines refer to various degrees of correlations in the disorder, as in Fig. 8: a solid line for uncorrelated disorder, dashed line for minimal value of p_{BC}, and short-dashed line for maximal value of p_{BC}. In all three cases, there is the same disorder in the coupling constants. Clearly, this type of (polarizability) disorder has a strong effect on this quantity. Simulations indicate that the strong increase in linewidth probably comes mostly from changes in the tails of the line rather than in a change of the full width at half maximum, which remains quite weakly dependent on the disorder in f for the values studied in Fig. 9.

[1]F. J. Dyson, Phys. Rev. **92**, 1331 (1953).
[2]L. B. Coleman, M. J. Cohen, M. J. Sandmann, D. J. Yamagishi, A. F. Garito, and A. J. Heeger, Solid State Commun. **12**, 1125 (1973); John Ferraris, D. O. Cowan, V. V. Walatka, and J. H. Perlstein, J. Am. Chem. Soc. **95**, 948 (1973).
[3]D. Jérome and H. J. Schulz, Adv. Phys. **31**, 299 (1982).
[4]J. M. Lopez Castillo and A. M. S. Tremblay, Phys. Rev. B **34**, 8482 (1986).
[5]S. Furuseth, L. Brattas, and A. Kjekshus, Acta Chem. Scand. **A29**, 623 (1975).
[6]S. Jandl, M. Banville, and J. Y. Harbec, Phys. Rev. B **22**, 5697 (1980).
[7]S. Jandl and J. Deslandes, Phys. Rev. B **24**, 1040 (1981).
[8]J. Deslandes and S. Jandl, Phys. Rev. B **30**, 6019 (1984).
[9]R. Provencher, S. Jandl, and C. Carlone, Phys. Rev. B **26**, 7049 (1982).
[10]C. Deville-Cavellin and S. Jandl, Solid State Commun. **33**, 813 (1980).
[11]S. Jandl, C. Deville-Cavellin, and J. Y. Harbec, Solid State Commun. **31**, 351 (1979).
[12]J. Y. Harbec, C. Deville-Cavellin, and S. Jandl, Phys. Status Solidi B **96**, K117 (1979).
[13]A. Grisel, F. Levy, and T. J. Wieting, Physica B+C **99B**, 365 (1980).
[14]T. J. Wieting, A. Grisel, F. Lévy, and Ph. Schmid, in *Proceedings of the International Conference on Quasi-One-Dimensional Conductors, Dubrovnik* (Springer-Verlag, Berlin, 1979), Vol. I, p. 354.
[15]C. Sourisseau and Y. Mathey, Chem. Phys. **63**, 143 (1981).
[16]A. Zwick, M. A. Renucci, and A. Kjekshus, J. Phys. C **13**, 5603 (1980).
[17]P. Gard, C. Sourisseau, and O. Gorochov, Phys. Status Solidi B **144**, 885 (1987).
[18]S. P. Gwet, Y. Mathey, and C. Sourisseau, Phys. Status Solidi B **123**, 503 (1984).
[19]A. Zwick, G. Landa, M. A. Renucci, and R. Carles, Phys. Rev. B **26**, 5694 (1982).
[20]G. Nouvel, A. Zwick, M. A. Renucci, and A. Kjekshus, Phys. Rev. B **32**, 1165 (1985).
[21]R. Gagnon, S. Jandl, and M. Aubin, J. Phys. Condens. Matter **1**, 1329 (1989).
[22]C. Deville-Cavellin, G. Martinez, O. Gorochov, and A. Zwick, J. Phys. C **15**, 5371 (1982).
[23]Splittings are equal in ZrS_3 under 70 kbar and in $Zr_{0.2}Hf_{0.8}S_3$, giving an indication of the substitution equivalent of hydrostatic pressure.
[24]In two other studies of trichalcogenides solid solutions $ZrS_{3-x}Se_x$ (Ref. 25) and $Zr_{1-x}Ti_xS_3$ (Ref. 17), it was mentioned that low-frequency phonons are governed by interchain long-range forces and exhibit a one-mode behavior while internal chain deformation modes at higher frequencies imply shorter-range forces and show a two-mode behavior. Such a trend is not confirmed in $Zr_{1-x}Hf_xS_3$. Low-frequency Ag modes (lines 6,7,8) behave as a two-mode type whereas high-frequency Ag modes (lines 1–5) and all the Bg modes exhibit a one-mode type. Much emphasis has been put (Refs. 27 and 28) in the past on the distinction between one-mode- and two-mode-type behavior. Nevertheless, it is known (Refs. 28 and 29) that both one- and two-mode behaviors can be observed in one-dimensional chains. Our measurements combined to those of Refs. 17 and 25 confirm that in the quasi-one-dimensional trichalcogenide systems both behaviors are observed.
[25]A. Zwick, G. Landa, R. Carles, M. A. Renucci, and A. Kjekshus, Solid State Commun. **45**, 889 (1983).
[26]With central forces only between metal ion and S_3 triangular arrangement, longitudinal motion of the S_3 complex also implies small transverse motion of the sulfur ions, which we assume can be neglected.
[27]I. F. Chang and S. S. Mitra, Adv. Phys. **20**, 359 (1971).
[28]A. S. Barker and A. J. Sievers, Rev. Mod. Phys. **47**, Suppl. 2, S1 (1975).
[29]J. M. Lopez Castillo and A. M. S. Tremblay, Phys. Rev. B **33**, 6599 (1986).
[30]G. P. Srivastava, José Luis Martins, and Alex Zunger, Phys. Rev. B **31**, 2561 (1985).
[31]A. Gomyo, T. Suzuki, and S. Iijima, Phys. Rev. Lett. **60**, 2645 (1988).
[32]Th. M. Nieuwenhuizen and J. M. Luck, J. Stat. Phys. **48**, 393 (1987); B. I. Halperin, Phys. Rev. **139**, A104 (1965).